scientific reports

Check for updates

OPEN

Poneratoxin as a key tool for investigating the relationship between sodium channel hypersensitivity and impaired nerve cell function

Zirui Lü, Xiandong Dai, Jianjie Xu, Mu Zhu, Bo Chen, Yongbiao Guo, Zhenhua Gao & Fanhua Meng✉

Poneratoxin (PoTX) is a 25-residue peptide derived from the venom of bullet ant, *Paraponera clavata*, recognized for its potent activation of Na_V channel and pain-inducing effects in murine models. In this study, for the first time, we conducted the evaluation of the excitotoxicity of PoTX and performed an in-depth analysis of transcriptomics and proteomics in vitro to elucidate its impact on the nervous system and underlying pharmacological mechanisms. Our results demonstrated that PoTX significantly induced calcium accumulation in SH-SY5Y cell model. Transcriptomic and proteomic analyses revealed that PoTX treatment led to cell cycle arrest, reduced neuronal plasticity, and accelerated cellular senescence. Additionally, PoTX significantly increased tau protein phosphorylation and aggregation via PI3K-Akt-mediated activation of GSK-3 and upregulation of CDK5. It also impaired autophagy by inhibiting ULK1 expression and activity, while concurrently downregulating multiple proteins associated with neuronal excitability. Given these findings and the high tolerance of nerve cells to PoTX treatment alone, along with its potent and sustained activation of Na_V channels, PoTX may serve as a valuable tool for investigating the pharmacological relationship between hypersensitivity of Na_V channels and the progression of neurological disorders, thereby facilitating the identification of potential therapeutic targets and corresponding drug development.

Keywords Poneratoxin, Transcriptomics, Proteomics, Neurological disorders

The family of voltage-gated sodium channels (VGSCs), as the primary mediators in action potential generation, is considered to play a crucial role in the establishment and stabilization of cellular electrophysiological functions[1]. They are constituted by the pore-forming α-subunit (of ~ 260 kDa), which is essential and sufficient for channel functions, along with accessory β-subunits of smaller size (30–40 kDa) that modulate gating, kinetics, and channel surface density[2]. The α-subunits of VGSCs consist of nine isoforms ($Na_V1.1$-$Na_V1.9$), which are encoded in humans by a family of nine highly conserved genes (*SCNA1-5*, *SCNA7-10*)[3]. Among them, $Na_V1.1$, $Na_V1.2$, $Na_V1.3$, and $Na_V1.6$, encoded respectively by *SCN1A*, *SCN2A*, *SCN3A*, and *SCN8A*, represent the principal Na_V channels expressed in the central nervous system and play essential roles in the initiation and propagation of action potentials as well as neural network activity[4].

A diverse range of neurological disorders, including epilepsy, migraine, neurodegenerative diseases and neuropathic pain, is characterized by abnormal neuronal excitability. Although the specific pathological mechanisms necessitate further in-depth investigation, an increasing body of evidence suggests that VGSCs, as key determinants of intrinsic neuronal excitability, exhibit abnormal expression and function that are closely associated with the progression of these conditions[2,5]. For instance, the recent study utilizing primary hippocampal neurons has identified the overexpression of $Na_V1.6$ induced by Aβ1-42 oligomers as a key factor contributing to neuronal hyperexcitability in Alzheimer's diseasea mouse model[6]. Therefore, investigating the relationship between functional abnormalities of VGSCs and neurological disorders is of great significance for

State Key Laboratory of Chemistry for NBC Hazards Protection, Beijing 102205, China. ✉email: mengfanhua@sklnbcpc.cn

understanding the underlying pathological mechanisms, identifying suitable therapeutic targets, and facilitating drug development efforts.

Specific modulators are considered powerful tools for elucidating the pharmacological functions and structure of target proteins[7]. The stings of bullet ant, *Paraponera clavata* (subfamily Paraponerinae) found in the tropical regions of Central and South America, can induce uncontrollable tremors and intimidate severe localized pain that may persist for several hours[8]. With respect to study of the toxic components, Piek and his colleagues isolated and identified a 25-residue disulphide-free peptide, poneratoxin (PoTX) from the venom of bullet ants[9], which has been shown to stimulate skeletal muscle fibers in frogs and rats[10] through a previously undescribed mechanism[11]. More recently, Robinson et al. revealed that PoTX can directly modulate the activity of VGSCs, reduce the voltage threshold for activation of subtypes $Na_V1.6$ and 1.7 and inhibit their inactivation, with the EC_{50} values of 0.097 ± 0.010 and 2.3 ± 0.4 μM, respectively, in whole-cell voltage-clamp electrophysiology assay[12]. However, further comprehensive investigation is needed to clarify the binding site of PoTX on Na_V channels, understand the mechanisms underlying continuous channel activation, and explore its pharmacological effects on neuronal cells.

In this study, we verified that apart from its agonistic activity on $Na_V1.6$ and 1.7, PoTX served as a potent agonist for $Na_V1.2$ and 1.3 subtypes. Building upon this finding, we systematically evaluated the membrane potential activation and neurotoxic effects of PoTX in SH-SY5Y cells. The results indicated that PoTX could directly modulate the membrane excitability, remarkably enhance sodium influx, thereby resulting in the accumulation of intracellular Ca^{2+}. However, treatment with PoTX alone did not significantly impact cell viability. Furthermore, a comprehensive analysis combining transcriptomics and proteomics revealed that PoTX significantly induced the activation of cell cycle arrest and senescence pathways in SH-SY5Y cells. Concurrently, it regulated the expression, abundance, or modification of a series of proteins associated with neurodegenerative diseases. Notably, these effects could be abrogated by the Na_V channel blocker tetrodotoxin (TTX). Identical pharmacological effects were also witnessed in ND7/23 cells. Collectively, these findings confirmed that the pharmacological effects elicited by PoTX are predominantly mediated by the activation of Na_V channels. As a potent and persistent agonist of Na_V channels that does not substantially affect cell viability, PoTX holed great promise as a powerful tool molecule. It can be employed to delve deeper into the compensatory mechanisms of nerve cells in response to continuous Na_V channels activation and calcium toxicity, as well as to explore the intricate relationship between abnormal sodium channel function and various neurological disorders.

Results

In vitro assessment of excitotoxicity of PoTX

To begin with, a systematic evaluation was conducted on the excitotoxicity of PoTX based on SH-SY5Y cells, as they are considered a widely utilized human cell mode for neuroscience investigation, including neurotoxicity of agents[13], Parkinson's disease[14], Alzheimer's disease[15], inflammation[16], and ischemia[17]. Electrophysiological studies revealed that, in addition to the previously validated $Na_V1.6$ and $Na_V1.7$ subtypes[12], PoTX exhibited substantial agonistic activity toward two additional endogenously expressed subtypes, $Na_V1.2$ and $Na_V1.3$, in SH-SY5Y cells[18], with EC_{50} values of 0.41 ± 0.033 μM and 1.04 ± 0.015 μM, respectively (Fig. 1A). Meanwhile, treatment with PoTX significantly modified the voltage-dependent sodium channel current patterns in SH-SY5Y cells (Fig. 1B). It slowed the inactivation kinetics of sodium channels (Fig. 1C), reduced the peak current amplitude (Fig. 1D), and induced a rapid and sustained increase in intracellular Ca^{2+} levels (Fig. 1E). Notably, even following the removal of PoTX, a 24-h exposure of SH-SY5Y cells to PoTX at concentrations of 1 μM and 10 μM led to persistent changes in membrane excitability, as demonstrated by a significant reduction in voltage-activated peak current (Fig. 1F). Collectively, these results suggested that PoTX treatment exerted a profound influence on the excitability of SH-SY5Y cells.

Furthermore, we evaluated the excitotoxicity of PoTX by by CCK-8 assay. The results indicated that PoTX treatment alone did not significantly reduce cell viability, even at a concentration of 40 μM for 24 h (Fig. 1G). Similar results were observed in ND7/23 cells (Fig. 1H), a fusion cell-line of mouse N18Tg2 neuroblastoma and embryonic rat DRG that abundantly expressed $Na_V1.6$ and $Na_V1.7$ channels[19]. This indicated that although PoTX exhibited more pronounced agonistic activity on $Na_V1.6$ channels, its solitary action did not precipitate a substantial decline in the viability of cells with high $Na_V1.6$ expression. This resilience may be attributed to the counteracting effect of Na^+/K^+-ATPase on the rising intracellular Na^+ level[21,22]. Accordingly, we developed a SH-SY5Y cell-based model through ouabain (OB) intervention to enhance the sensitivity of the model to Na^+ influx toxicity. OB is a specific inhibitor of Na^+/K^+-ATPase that is responsible for blocking the efflux of Na^+/K^+-ATPase to overloaded Na^+ intracellularlly[23]. When cells exposed to OB and Na_V channel activator, excessive opening of Na_V channels would lead to cell swelling and death[23]. Veratridine (VTD), a well-established Na_V channel agonist serves as a positive control for model construction and method validation[24].

Firstly, we conducted an investigation into the influence of treating SH-SY5Y cells with diverse concentrations of OB independently for time periods of 3, 6, 9, 12–24 h (Fig. S1A–E) on cell viability. The experimental outcomes revealed that upon extending the treatment period to 24 h, the impact of OB on cell viability reached a relatively stable state and manifested an obvious dose-dependent pattern (Fig. S1E). Consequently, a treatment duration of 24 h was chosen for further exploration of the optimal concentration of OB intervention. Concurrently, in order to attenuate the toxic effects of OB, four concentrations of OB treatment, under which cell viability was maintained above 50% (0.2, 0.1, 0.05, and 0.025 μM, as presented in Fig. S1E), were selected for the subsequent combined administration analysis in conjunction with VTD. Eventually, considering that VTD treatment induced a more significant reduction in cell viability under such circumstances, the combination of 0.1 μM OB and Na_V channel activator exposure for 24 h (Fig. 1I) was determined as the treatment condition for the evaluation model of excitatory cytotoxicity. According to the aforementioned model, VTD demonstrated a moderate degree of excitatory cytotoxicity in SH-SY5Y cells, with an IC_{50} value around 66 μM (Fig. 1J). This is

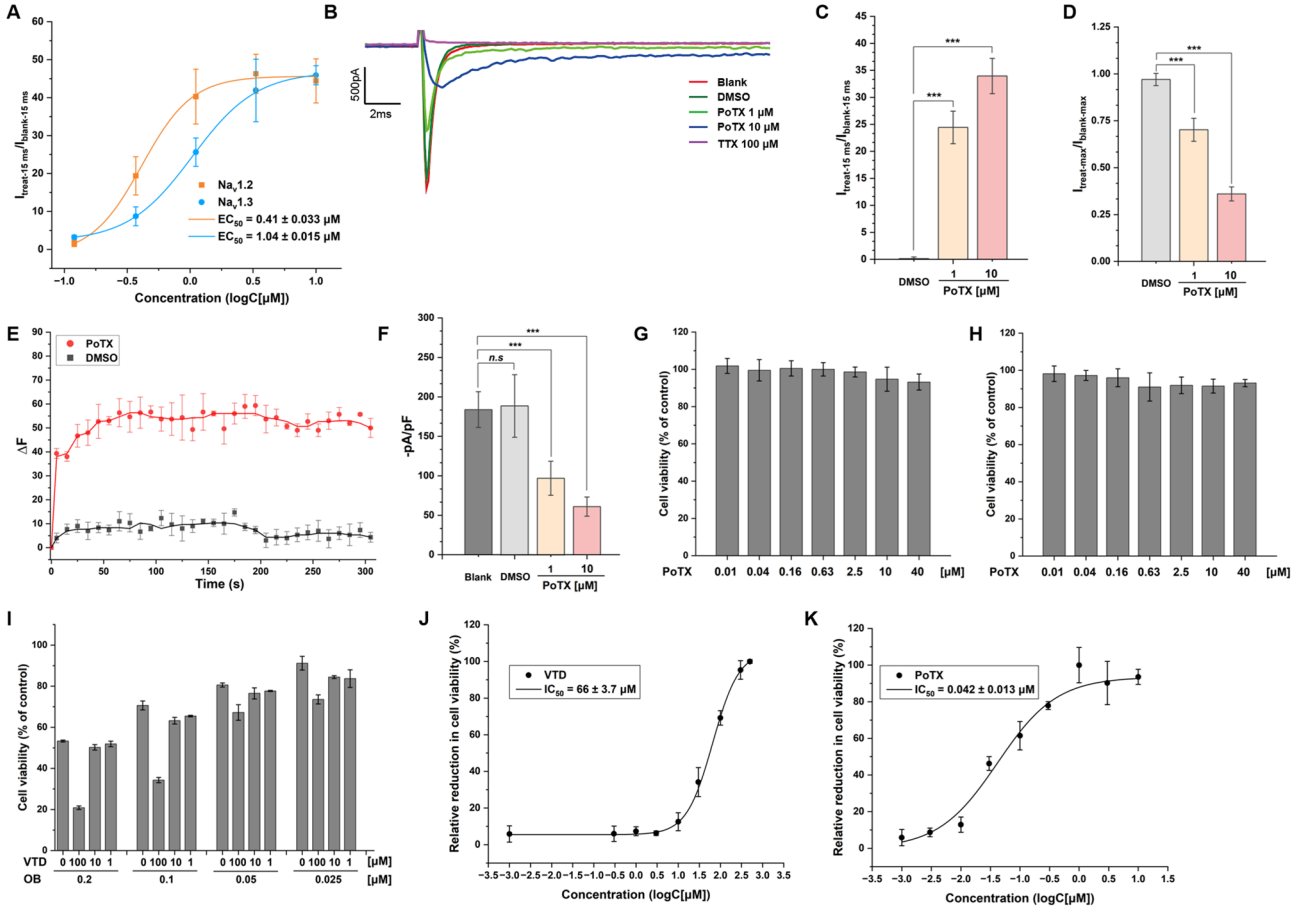

Fig. 1. Assessment of the excitotoxic effects of PoTX. (**A**) Concentration-response relationships for PoTX modulation of human $Na_V1.2$ and $Na_V1.3$ ($n = 3$ cells), where response is [(current amplitude at 15 ms after treatment ($I_{treat\text{-}15\ ms}$)/current amplitude at 15 ms before treatment ($I_{blank\text{-}15\ ms}$)]. (**B**) Representative sodium channel current response to a step depolarization from − 100 to − 10 mV in the absence and presence of PoTX (1 μM or 10 μM) based on SH-SY5Y cells. The treatment of 100 μM tetrodotoxin (TTX) was used as a control to block the current. (**C**) Sodium channel sustained current (current amplitude at 15 ms) evoked by a step depolarization from − 100 to − 10 mV before ($I_{blank\text{-}15\ ms}$) and after treatment with DMSO or indicated concentrations of PoTX ($I_{treat\text{-}15\ ms}$) based on SH-SY5Y cells ($n = 4$ cells), expressed as the fold of $I_{treat\text{-}15\ ms}/I_{blank\text{-}15\ ms}$. (**D**) Sodium channel peak current evoked by a step depolarization from − 100 to − 10 mV before ($I_{blank\text{-}max}$) and after treatment with DMSO or indicated concentrations of PoTX ($I_{treat\text{-}max}$) based on SH-SY5Y cells ($n = 4$ cells), expressed as the fold of $I_{treat\text{-}max}/I_{blank\text{-}max}$. (**E**) The curve of the variation in the fluorescence signal of intracellular Ca^{2+} in SH-SY5Y cells after treatment with DMSO or 10 μM PoTX. (**F**) The relative peak current density evoked by a step depolarization from − 100 to − 10 mV in SH-SY5Y cells after treatment with DMSO or the indicated concentrations of PoTX for 24 h ($n = 4$ cells). The viability of (**G**) SH-SY5Y or (**H**) ND7/23 cells following treatment with indicated concentrations of PoTX alone for 24 h. The viability of SH-SY5Y cells following treatment with indicated concentrations of OB in combination thereof with indicated concentrations of VTD for 24 h. Dose-response curve of (**J**) VTD or (**K**) PoTX against growth of SH-SY5Y cells combined with 0.1 μM OB. Cell viability was measured by CCK-8 assay and mean values of triplicates ± SD are shown. Representative results of three independent experiments are shown. Significance analysis of normally distributed data with variance similar between groups used two-tailed Student's t test. *n.s* no significant difference, $^*p < 0.05$; $^{**}p < 0.01$; $^{***}p < 0.001$.

in accordance with its reported Na_V channel agonist activity[25]. Notably, PoTx exhibited remarkable excitatory toxicity, with an IC_{50} value reaching as low as 0.042 μM (Fig. 1K), which is three orders of magnitude greater than that of VTD.

Meanwhile, cytological experiments demonstrated that subsequent to the combined treatment of PoTX and OB, a notable swelling and rounding of the morphological features of SH-SY5Y cells were observed (Fig. 2A). And there was a substantial increase in the proportion of apoptotic cells, particularly those in the early apoptotic stage (Fig. 2B,C). The results as presented above suggested that PoTX can efficiently activate the Na_V channels and trigger the accumulation of intracellular Ca^{2+} in SH-SY5Y cells, thereby leading to significant excitotoxicity when the cellular compensatory mechanisms are compromised.

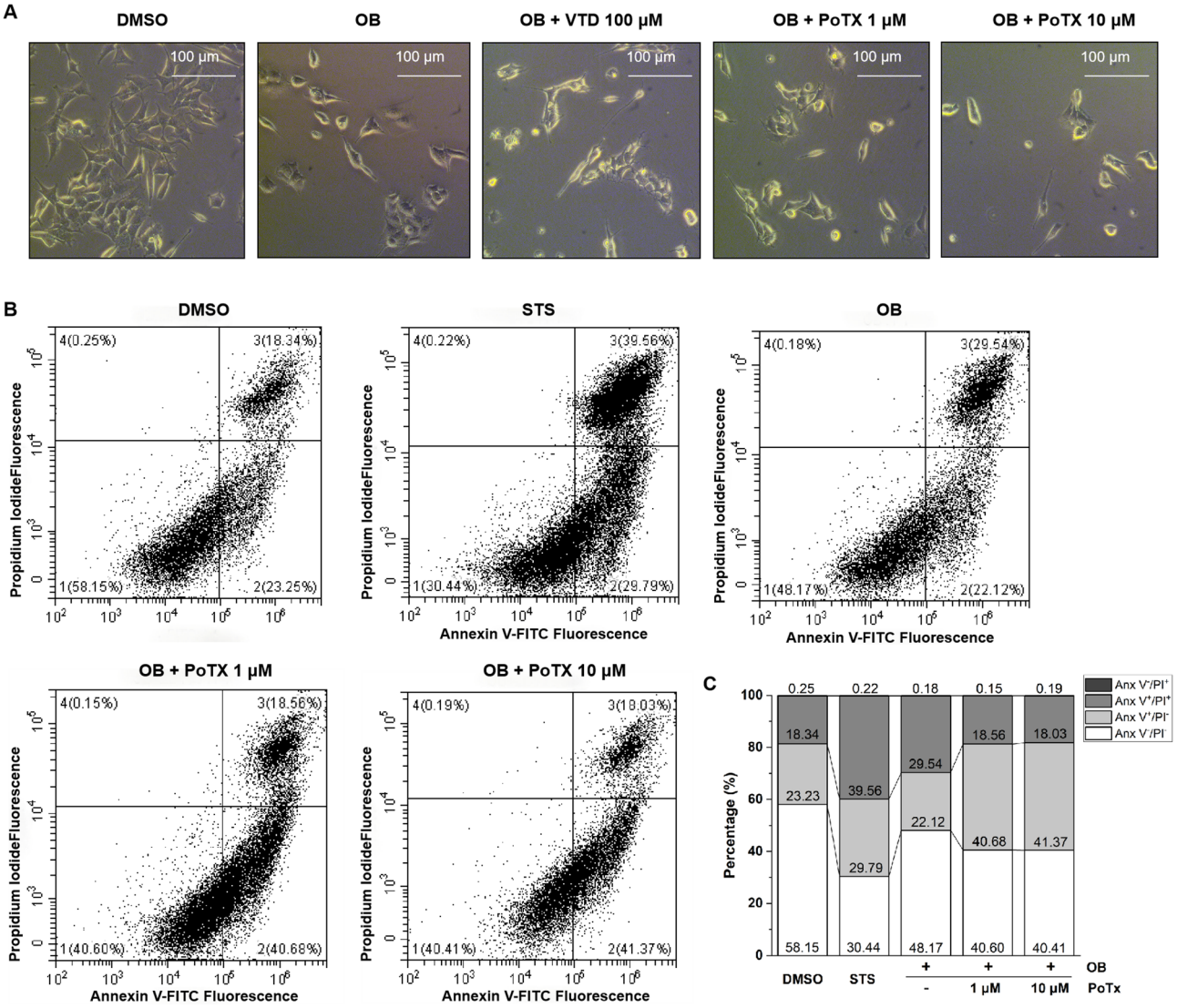

Fig. 2. The effects of PoTX on the morphology and apoptosis of SH-SY5Y cells. (**A**) The bright field images of SH-SY5Y cells treated with DMSO, OB (0.1 μM) alone or in combination thereof with indicated concentrations of VTD or PoTX for 24 h. (**B**) Percentages of cells in different apoptotic states measured by flow cytometric analysis. SH-SH5Y cells were treated with DMSO, staurosporine (STS, 50 nM), OB (0.1 μM) alone or OB (0.1 μM) in combination thereof with indicated concentrations of PoTX for 24 h. The cell apoptotic state was analyzed by double-staining with Annexin V-FITC and PI. (**C**) Percent stacked column chart of different apoptotic states in Fig. 2B. Data are representative of three independent experiments.

Transcriptomic analysis on the underlying mechanisms of PoTX-induced nerve injury

Global analysis

To further investigate the potential pharmacological impacts of PoTX on the nervous system, the transcriptomic alterations within SH-SY5Y cells were meticulously analyzed after 24 h of treatment with either a high concentration (10 μM, High group) or a lower concentration (1 μM, Low group) of PoTX. All sequencing data underwent strict quality control and standardization before analysis. As shown in Table 1, an average of 45 million raw reads were obtained from control and two test groups. After the quality control and contamination removal, over 98% of the high-quality clean reads were available for assembly and further analysis. The clean reads were mapped to the human reference genome, and the mapping ratios of each group were higher than 95%, indicating the adequate data quality for each groups that could be used for subsequent analyses.

Principal component analysis (PCA) showed that the samples in each group had sound clustering, and the distance between the samples in the control group and the two test groups was significantly higher than that between the two test groups with different concentrations (Fig. 3A). The adjusted P-value (P-adjust) < 0.05 and Fold Change (FC) ≥ 2 were adapted as the screening criterion. As indicated by the results of the volcano plot depicted in Fig. 3B, a total of 335 genes were identified as differentially expressed genes (DEGs) in the Low group when compared with the Control group. Among these DEGs, there are 119 up-regulated genes and 216 down-

Sample	Raw reads	Clean reads	Total mapped	Multiple mapped	Uniquely mapped
Control_1	45,114,556	44,612,214	43,402,540 (97.29%)	3,201,149 (7.18%)	40,201,391 (90.11%)
Control_2	44,790,734	44,316,536	43,161,383 (97.39%)	3,124,195 (7.05%)	40,037,188 (90.34%)
Control_3	47,568,152	47,059,156	45,827,622 (97.38%)	3,371,954 (7.17%)	42,455,668 (90.22%)
Low_1	45,386,102	44,858,328	43,700,637 (97.42%)	3,224,121 (7.19%)	40,476,516 (90.23%)
Low_2	42,771,000	42,326,804	41,193,131 (97.32%)	3,004,164 (7.10%)	38,188,967 (90.22%)
Low_3	48,672,076	48,141,090	46,863,063 (97.35%)	3,407,396 (7.08%)	43,455,667 (90.27%)
High_1	41,856,060	41,403,602	40,305,735 (97.35%)	2,933,277 (7.08%)	37,372,458 (90.26%)
High_2	48,824,620	48,175,136	46,826,639 (97.20%)	3,459,030 (7.18%)	43,367,609 (90.02%)
High_3	44,335,732	43,847,568	42,685,179 (97.35%)	3,163,743 (7.22%)	39,521,436 (90.13%)

Table 1. Trimming and read mapping results of the sequences generated from SH-SY5Y cells with or without PoTX treatment. Control represents SH-SY5Y cells without PoTX treatment; low represents SH-SY5Y cells with 1 μM PoTX treatment for 24 h; high represents SH-SY5Y cells with 10 μM PoTX treatment for 24 h. Three replicates of control (control_1, _2, _3), PoTX of 1 μM (Low_1, _2, _3) and 10 μM (High_1, _2, _3) treatments were carried out in RNA-seq analysis.

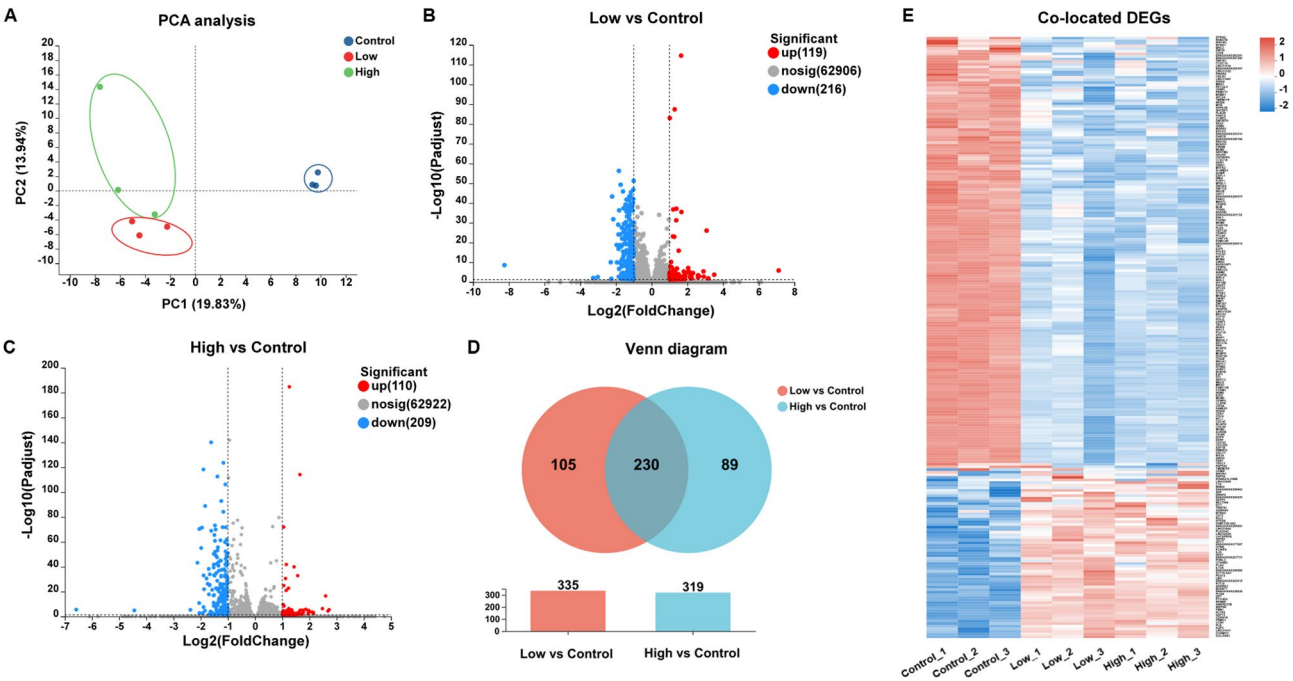

Fig. 3. RNA-seq analysis of SH-SY5Y cells with or without PoTX treatment. (**A**) Principal component analysis (PCA) of transcriptome among the Control, Low and High groups. Volcano plots of the gene changes in the (**B**) Low and (**C**) High group when compared with the Control group. (**D**) Venn diagram analysis of DEGs among the Low and High groups. (**E**) Heatmap of the expression levels of co-located DEGs in the Low and High group. The red represents higher expression levels of genes, while blue represents lower expression levels. Control represents SH-SY5Y cells without PoTX treatment; Low group represents SH-SY5Y cells with 1 μM PoTX treatment for 24 h; High group represents SH-SY5Y cells with 10 μM PoTX treatment for 24 h. Three replicates of each group were carried out.

regulated genes. In the High group, totally 319 DEGs were detected, of which 110 DEGs were up-regulated and 209 DEGs were down-regulated compared with the Control group (Fig. 3C). No DEGs can be found between the Low group and High group (Fig. S2). Based on gene expression matrix, the Venn diagram was employed to analyze the co-located and specifically located DEGs among the Low and High groups. As shown in Fig. 3D, approximately 70% of the DEGs (230) were shared between the two test groups, and exhibited the same trend of change (Fig. 3E). For the DEGs specifically expressed in a single test group, despite no significant, generally the same trend of change can also be observed in another group (Fig. S3A,B). Collectively, the aforementioned results demonstrated the sufficient reliability and representativeness of transcriptome differential analysis, which can be utilized for further functional and pharmacological investigations.

Functional annotation and enrichment analysis

The results of GO (Gene Ontology) enrichment analysis on the acquired DEGs demonstrated that, irrespective of whether it was treated with a low ((Fig. 4A) or high (Fig. S4A) concentration, PoTX conspicuously influenced the gene expressions related to the cell cycle, DNA replication, and damage repair within SH-SY5Y cells. Similarly, the KEGG (Kyoto Encyclopedia of Genes and Genomes) enrichment analysis identified multiple pathways associated with cell proliferation suppression, such as cell cycle, DNA replication, homologous recombination, cellular senescence and p53 patway (Fig. 4B, Fig. S4B). Further KEGG functional annotation analysis of the co-localized DEGs in the Low and High groups revealed that PoTX significantly inhibited the cell cycle, DNA replication, and the p53 signaling pathway (Fig. 4C,E) and induced the activation of the cell senescence pathway (Fig. 4F). In addition, it seemed that the activity of the PI3K-Akt pathway was significantly suppressed in both treatment groups, as evidenced by the down-regulation of *MYB*, *BRCA1*, *CCNE*, alongside an up-regulation of *CDKN1A* (Fig. 4G). To validate the findings from RNA-seq analysis, 5 DEGs within the aforementioned pathways were selected for qRT-PCR analysis to further elucidate their expression profiles. The results of 5 genes in expression measured by qRT-PCR showed similar alterations to those identified by RNA-Seq analysis, including an up-regulated gene (*CDKN1A*) and 4 down-regulated genes (*MCM4*, *E2F1*, *FEN1* and *RRM2*, Fig. 4H), confirming the reliability of the RNA-seq analysis results. Moreover, the pronounced up-regulation of Ca^{2+}-dependent phospholipase A2 (*PLA2G4C*, Fig. 4H), a rate-limiting enzyme involved in the synthesis of bioactive lipid mediator arachidonic acid[26]and cytochrome c oxidase subunit 6B2 (*COX6B2*, Fig. 4H), a critical component of mitochondrial respiratory chain complex IV[27]genes expression suggested that intracellular calcium overload induced by PoTX have contributed to mitochondrial dysfunction and lipid metabolism dysregulation. These factors represented significant risk determinants for long-term depression, cognitive disorder and neurodegenerative diseases such as Alzheimer's disease, Huntington disease and amyotrophic lateral sclerosis[28–30].

Then, we conducted a partial validation of the transcriptional regulatory effects of PoTX using the ND7/23 cell line. As illustrated in Fig. 5A and C, PoTX induced comparable alterations in gene expression within ND7/23 cells, characterized by the up-regulation of *CDKN1A* and down-regulation of *MCM4* and *E2F1* expression

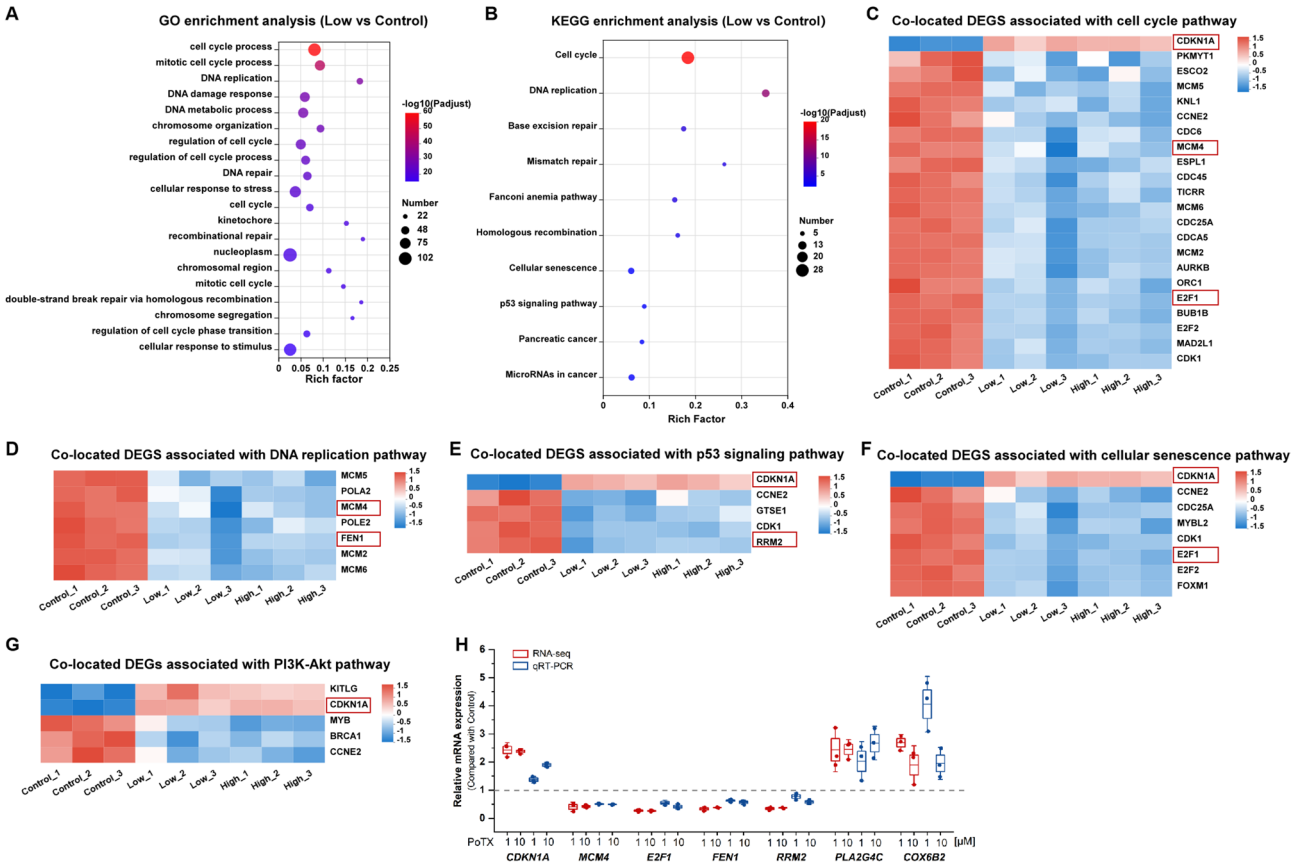

Fig. 4. Functional annotation and enrichment analysis of DEGs in the SH-SY5Y of Control and PoTX-treated groups. (**A**) GO and (**B**) KEGG enrichment analysis for DEGs in the Low group compared with Control group (P-adjust < 0.05). Heatmaps of the expression levels of co-located DEGs in the (**C**) cell cycle, (**D**) DNA replication, (**E**) p53 signaling, (**F**) cellular senescence and (**G**) PI3K-Akt pathway. The red represents higher expression levels of genes, while blue represents lower expression levels. (**H**) Relative mRNA expression of corresponding DEGs measured by qRT-PCR ($n = 3$) or RNA-seq analysis ($n = 3$). Data are expressed as the mean ± 1.96 SD.

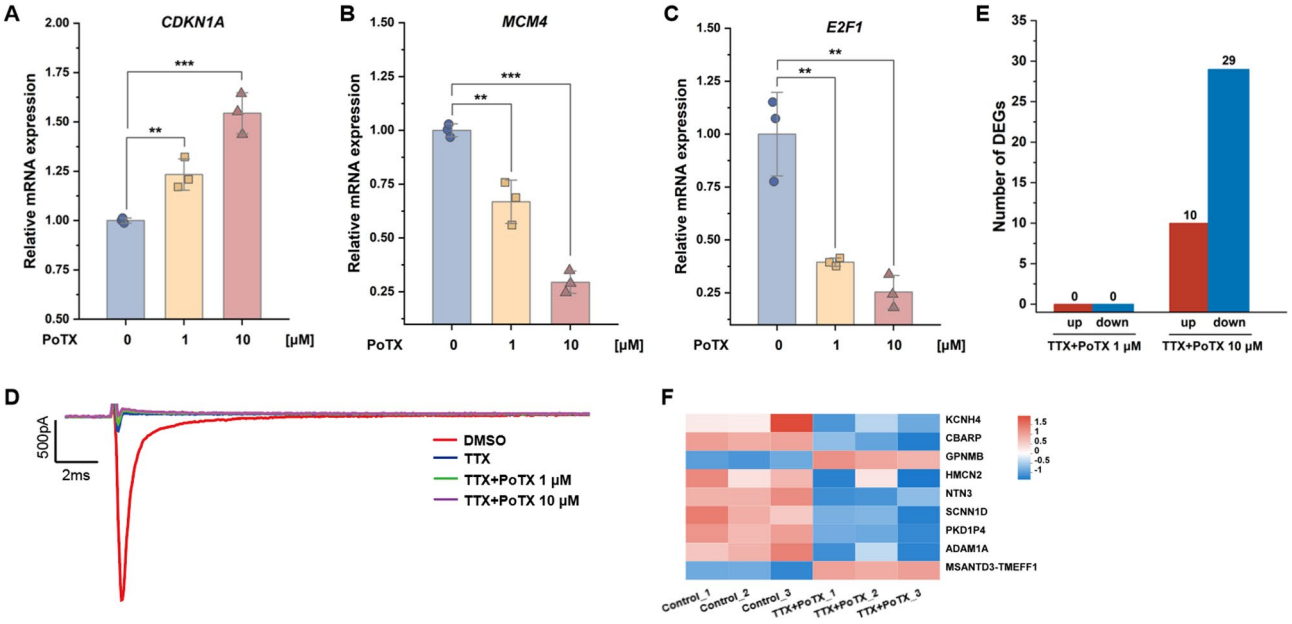

Fig. 5. Assessment of the expression levels of target genes induced by PoTX and the antagonistic impact of TTX on PoTX-induced transcriptomic alterations. Bar chart of changes in the expression levels of (**A**) *CDKN1A*, (**B**) *MCM4*, or (**C**) *E2F1* genes quantified by qRT-PCR ($n = 3$) after 24-h treatment with DMSO or indicated concentrations of PoTX in ND7/23 cells. (**D**) Representative sodium channel current response to a step depolarization from − 100 to − 10 mV in the absence and presence of PoTX (1 μM or 10 μM) in combined with 100 μM TTX based on SH-SY5Y cells. (**E**) Bar chart of the number of DEGs in SH-SY5Y cells treated with 1 μM or 10 μM PoTX combined with 100 μM TTX for 24 h, compared with the Control group. (**F**) Heatmap of the expression levels of DEGs associated with membrane proteins or membrane protein complexes. Control represents SH-SY5Y cells with DMSO treatment; TTX + PoTX represents SH-SY5Y cells with 10 μM PoTX and 100 μM TTX combined treatment for 24 h. The red represents higher expression levels of genes, while blue represents lower expression levels. Significance analysis of normally distributed data with variance similar between groups used two-tailed Student's *t* test. $^{**}p < 0.01$; $^{***}p < 0.001$.

levels. Additionally, we utilized tetrodotoxin (TTX), a potent inhibitor of $Na_V1.2$, 1.3, 1.6, and 1.7 channels[31], to block the activation of Na_V channels. Electrophysiological analysis revealed that treatment with 100 μM TTX completely abolished PoTX-induced membrane potential activation in SH-SY5Y cells (Fig. 5D). Under this condition, the transcriptomic alterations within SH-SY5Y cells induced by PoTX were re-evaluated. The results revealed that, following the blockade of Na_V channels by TTX, compared to the control group without any pharmacological intervention, treatment with 1 μM PoTX did not induce significant transcriptomic changes in SH-SY5Y cells. Even at a high concentration of 10 μM, only 39 DEGs were identified, comprising 10 up-regulated and 29 down-regulated genes (Fig. 5E), using P-adjust < 0.05 and $|\log_2 FC| \geq 1$ as the screening criteria. The GO functional annotation analysis revealed that 9 of the DEGs were associated with membrane proteins or membrane protein complexes (Fig. 5F). The aforementioned results demonstrated that Na_V channel activation mediates the transcriptomic regulation induced by PoTX, as its inhibitor effectively counteracted these changes. In addition to directly evoking nociceptive responses and disrupting neuroelectrophysiological functions, PoTX, acting as a potent Na_V agonist, can also accelerate nerve cell senescence, induce cognitive impairment and contribute to the onset and progression of neurodegenerative diseases.

Proteomic analysis on the underlying mechanisms of PoTX-induced nerve injury

Furthermore, with the aim of delving deeper into the influence of PoTX on nerve cells and validating as well as complementing the results obtained from the transcriptome analysis, the 4D-DIA quantitative proteomics analysis were conducted to assess the protein expression changes in SH-SY5Y cells following PoTX treatment. A total of 8,735 proteins were successfully identified and quantified. The Venn analysis indicated that the mRNAs expression of all these proteins were detected in the RNA-seq analysis (Fig. 6A). The thresholds for screening differentially expressed proteins (DEPs) were established as a fold change (FC) ≥ 1.2 for up-regulated DEPs and ≤ 0.83 for down-regulated DEPs, with a p-value of < 0.05. In comparison to the Control group, a total of 556 proteins were identified as DEPs in the Low group treated with 1 μM PoTX, of which 218 DEPs were up-regulated and 338 DEPs were down-regulated (Fig. 6B). In the High group treated with 10 μM PoTX, the number of DEPs reached 623, comprising 270 up-regulated DEPs and 353 down-regulated DEPs (Fig. 6B). The KEGG annotation of identified DEPs revealed that, in addition to proteins associated with cell growth, death and motility, PoTX treatment also led to changes in a variety of proteins related to neurodegenerative diseases (Fig. 6C,D), including Alzheimer's disease (AD), amyotrophic lateral sclerosis (ALS), Parkinson disease (PD), spinocerebellar ataxia (SCA) and Huntington disease (HD). In particular, a total of 26 neurodegenerative disease-related DEPs were

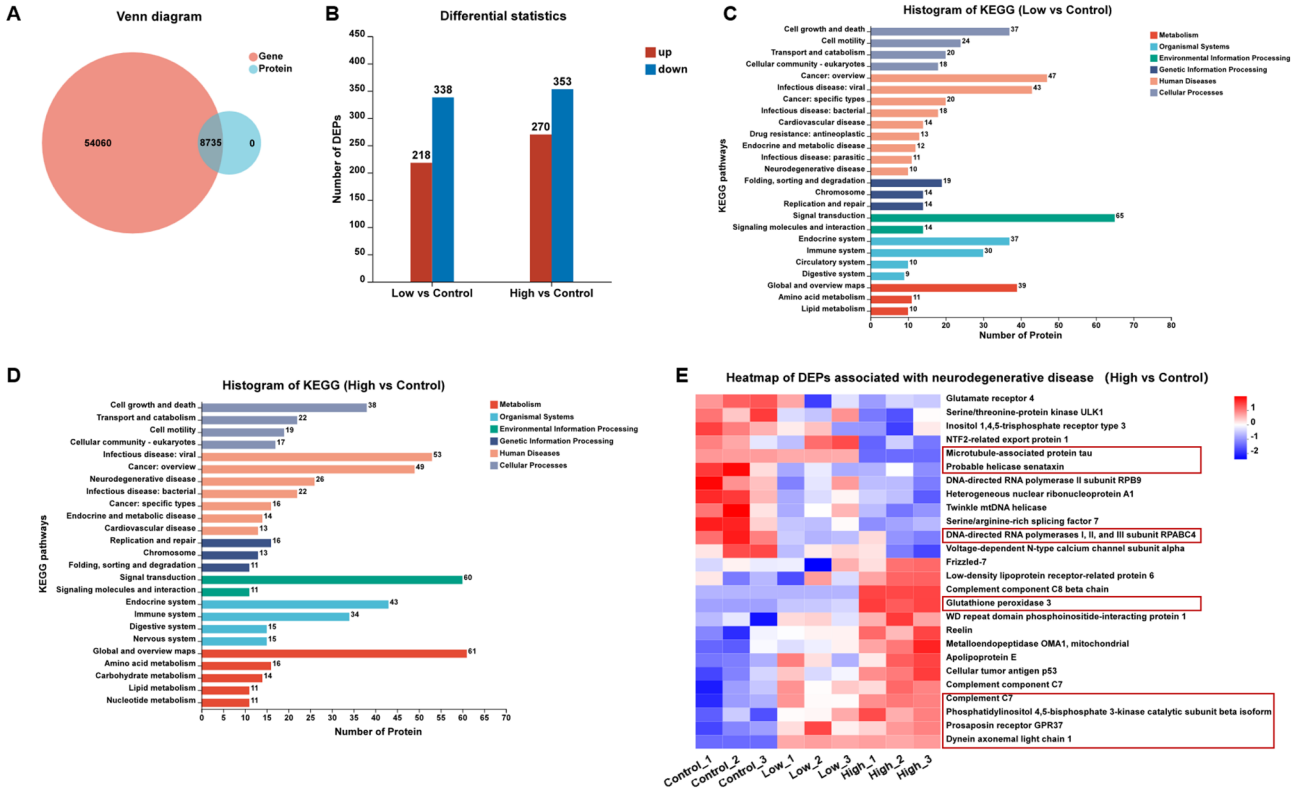

Fig. 6. Functional annotation analysis of DEPs in the SH-SY5Y of control and PoTX-treated groups. (**A**) Venn diagram analysis of identified genes and proteins in RNA-seq and quantitative proteomics analysis. (**B**) Bar chart of DEPs among the Low and High groups. Histogram of top 25 categories by number of DEPs annotated by KEGG analysis in the (**C**) Low and (**D**) High groups. (**E**) Heatmaps of the expression levels of DEPs associated with neurodegenerative diseases in the High group. The DEPs co-located in the Low group were marked with red frames. The red represents higher expression levels of genes, while blue represents lower expression levels.

identified in the High group (Fig. 6E). And in the Low group, there were 10 DEPs annotated as being associated with neurodegenerative diseases (Fig. S5), among which 8 DEPs were concurrently present in the High group (Fig. 6E).

It is notable that a variety of channel proteins implicated in neuronal excitability were down-regulated in SH-SY5Y cells following a 24-h treatment with PoTX at a concentration of 10 μM (Fig. 6E), including glutamate receptor 4 (GRIA4), voltage-dependent N-type calcium channel subunit alpha (CACNA1B) and inositol 1,4,5-trisphosphate receptor type 3 (ITPR3). Among them, several proteins, such as GRIA4, a subunit of the α-amino-3-hydroxy-5-methyl-4-isoxazole propionic acid (AMPA) receptor, have been shown to play a critical role in the neuroplasticity. And the decline of GRIA4 has been regarded as an important biomarker for the diagnosis of psychiatric disorders, like major depressive disorder, bipolar disorder, and schizophrenia[32]. For CACNA1B, the pore-forming subunit of the pre-synaptic neuronal voltage-gated calcium channel Cav2.2/N-type, its decrease of expression or the loss of function has also been documented to be correlated with HD[33], schizophrenia, behavioural and cognitive deficits[34]. Additionally, the elevated levels of apolipoprotein E (APOE) and low-density lipoprotein receptor-related protein 6 (LRP6) observed in High group were regarded as the high risk factors for multiple late-onset neurodegenerative diseases like PD, AD and HD[35,36].

What's more, the outcomes of proteomic analysis disclosed that the level of soluble microtubule-associated protein tau (tau) declined in both the Low and High groups (Fig. 6E, Fig. S5). Immunoblotting analysis indicated that apart from the reduction of soluble tau protein, the levels of phosphorylated tau protein at the Ser396 site and its polymers exhibited a significant increase (Fig. 7A), which is regarded as the principal marker and critical pathogenic factor for microtubule instability, neurofibrillary tangles, and tau protein-related neurodegenerative disorders such as AD[37]. Hence, we further probed into the biological mechanism of the elevated phosphorylation level of tau protein at the Ser396 site.

Glycogen synthase kinase-3 (GSK-3) and cyclin-dependent kinase 5 (CDK5) are two pivotal proteins that phosphorylate tau protein at Ser396[39]. The joint analysis of transcriptome and proteome demonstrated that in the category of Environmental Information Processing (EIP) within the KEGG annotation, irrespective of the Low or High groups (Fig. 7B,C), the PI3K-Akt pathway is the signaling pathway with the largest number of DEPs annotated. As a critical downstream element of the PI3K-Akt pathway, the activity of GSK-3 can be inhibited by Akt-mediated phosphorylation at Ser21 of GSK-3α and Ser9 of GSK-3[40,41]. Consequently, the phosphorylation

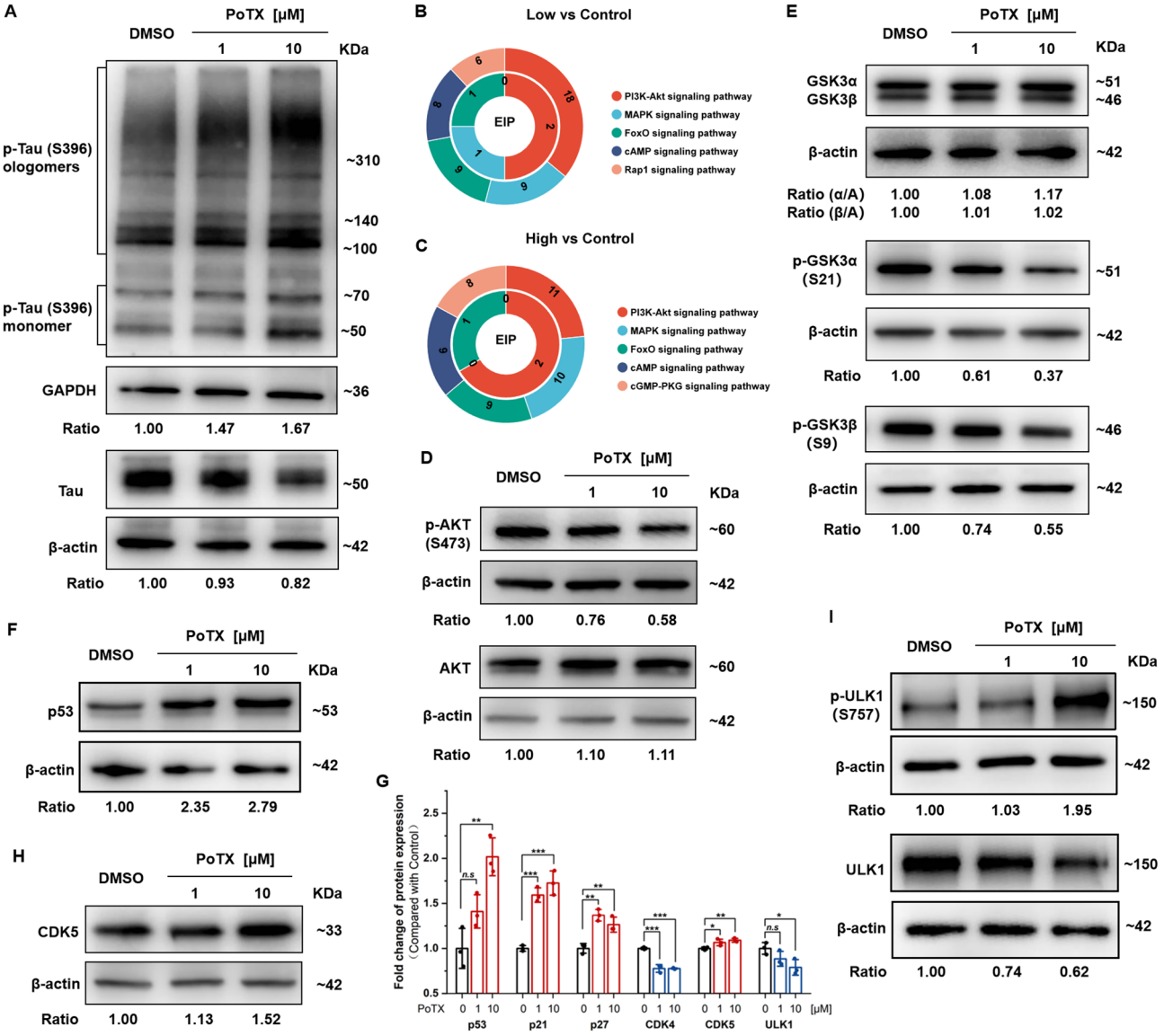

Fig. 7. Assessment of biomarker proteins related to neurodegenerative diseases after PoTX treatment in SH-SY5Y cells. (**A**,**D**–**F**,**H**–**I**) SH-SY5Y cells were treated with DMSO or indicated concentrations of PoTX for 24 h, followed by immunoblotting analysis with specific antibodies using total cell lysates. The expression levels of proteins were quantified using ImageJ software. Data are representative of three independent experiments. After joint analysis of transcriptome and proteome, the donut chart of the top 5 signaling pathways in the (**B**) Low and (**C**) High group with the largest number of DEPs in the Environmental Information Processing (EIP) category of KEGG, where the outer ring represents the number of DEPs and the inner ring represents the number of DEGs. (**G**) Bar chart of changes in the expression levels of target proteins measured by 4D-DIA quantitative proteomics analysis after PoTX treatment. Significance analysis of normally distributed data with variance similar between groups used two-tailed Student's t test. *n.s* no significant difference, $^{*}p < 0.05$; $^{**}p < 0.01$; $^{***}p < 0.001$.

levels of Akt and GSK-3 were analyzed via immunoblotting. As depicted in Fig. 7D,E, the treatment with PoTX did not give rise to conspicuous alterations in the total protein levels of Akt and GSK-3α/β. However, PoTX significantly inhibited the phosphorylation of Akt at Ser473 within SH-SY5Y cells (Fig. 7D). This, in turn, led to a reduction in Akt kinase activity[41] and consequently induced the suppression of the phosphorylation of downstream GSK-3α at Ser21 and GSK-3β at Ser9 (Fig. 7E), finally activating the kinase activity of GSK-3α/β. Meanwhile, consistent with the results of the aforementioned transcriptome analysis (Fig. 4G), the proteome analysis also revealed that the activity of the PI3K-Akt pathway underwent a significant downregulation subsequent to the PoTX treatment. This was embodied by the elevation of senescence-promoting related proteins, including cellular tumor antigen p53 (p53), cyclin dependent kinase inhibitor 1 A (p21), and cyclin dependent kinase inhibitor 1B (p27), along with the decline in the protein level of cyclin dependent kinase 4 (CDK4) (Fig. 7F,G). Additionally, although the increase was not statistically significant in the proteome analysis

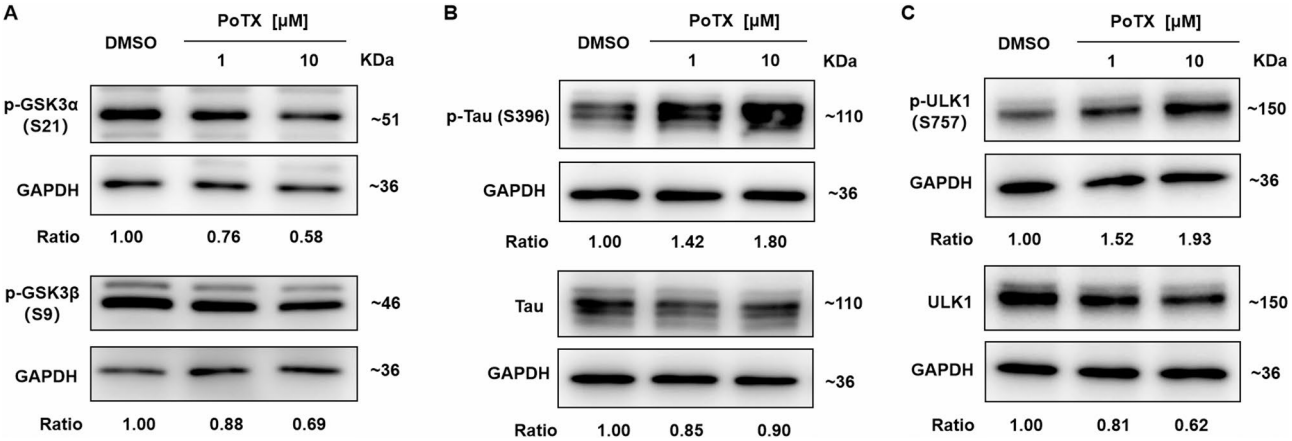

Fig. 8. Assessment of biomarker proteins related to neurodegenerative diseases after PoTX treatment in ND7/23 cells. (**A**–**C**) ND7/23 cells were treated with DMSO or indicated concentrations of PoTX for 24 h, followed by immunoblotting analysis with specific antibodies using total cell lysates. The expression levels of proteins were quantified using ImageJ software. Data are representative of three independent experiments.

(Fig. 7G), immunoblotting analysis indicated that PoTX could likewise induce the accumulation of CDK5 within SH-SY5Y cells (Fig. 7H), which would further enhance the phosphorylation level of tau protein at the Ser396.

Besides the elevated phosphorylation level of Tau protein, PoTX also notably influenced the expression of UNC-51-like kinase 1 (ULK1), which functions as a crucial convergence point for multiple signals that regulate autophagy[42]. Both proteomic and immunoblotting analyses results demonstrated that ULK1 experienced a significant reduction following PoTX treatment (Fig. 7G,I). Simultaneously, the phosphorylation level of Ser757 associated with the inhibition of its activity was remarkably increased (Fig. 7I). This implied that PoTX may accelerate the aging process of nerve cells and increase the risks of neurodegenerative diseases such as AD and PD through inhibiting autophagy[43].

The identical effects were also observed in ND7/23 cell line. As illustrated in Fig. 8A, following 24 h of PoTX treatment, the phosphorylation levels at Ser21 of GSK-3α and Ser9 of GSK-3β in ND7/23 cells were significantly reduced, indicative of enhanced kinase activity. Correspondingly, the phosphorylation level of tau protein, a crucial downstream substrate, exhibited a marked increase (Fig. 8B), which suggests an elevated risk of neurofibrillary tangle formation. In addition, in ND7/23 cells, PoTX treatment resulted in a marked decrease in the expression level of ULK1 kinase and a significant increase in the level of inhibitory phosphorylation (Fig. 8C). Despite the differences in the expression profiles of Na_V channel protein subtypes, the marker alterations observed in both ND7/23 and SH-SY5Y cells exhibited remarkable consistency. This consistency suggested that the PoTX-induced acceleration of neuronal aging may be linked to its long-term effects on membrane excitability. However, it remained unclear whether this effect is mediated by specific Na_V channel subtypes or directly results from changes in membrane potential.

In conclusion, proteomic analysis combined with immunoblotting experiments has shown that PoTX can significantly reduce neuronal plasticity and simultaneously induce the accumulation of neurotoxic substances and accelerate cellular senescence through the following mechanisms: (1) inducing tau protein phosphorylation and polymerization via PI3K-Akt pathway-mediated GSK-3 activation and up-regulation of CDK5 protein; (2) down-regulating the expression and activity of ULK1 protein to affect cellular autophagy; (3) down-regulating the expression of channel proteins related to neuronal excitability. Considering the substantial activation of Na_V channel and the subsequent multi-pathway effects, along with its minimal direct cytotoxicity, PoTX represented a highly promising tool for investigating the interplay between chronic pain, neuronal hypersensitivity with depression and various neurodegenerative diseases.

Discussion

PoTX, the algogenic substance isolated from the sting of the bullet ant, *Paraponera clavata*, has been established as a long-lasting agonist of Na_V channels. Nevertheless, its pharmacological effects on the nervous system have yet to undergo comprehensive evaluation. In this study, we systematically evaluated the excitotoxic effects of PoTX on nerve cells for the first time using the SH-SY5Y cell model. This human-derived cell model has been extensively utilized in neurodegenerative disease research due to its high relevance and applicability. Furthermore, the observed findings were independently validated through repeated experiments in ND7/23 cells. Our findings demonstrated that treatment with PoTX induced a marked change in both the excitability of the cell membrane and intracellular Ca^{2+} concentration, while not significantly affecting cell viability when used as a single agent. Under conditions of Na^+/K^+-ATPase inhibition, PoTX exhibited pronounced excitatory neurotoxicity, inducing morphological changes and apoptosis. Comprehensive transcriptomic and proteomic analyses revealed that PoTX can induce marked cell cycle arrest and senescence in neurons, accompanied by profound alterations in the expression of genes and proteins associated with neurodegenerative disorders. Additionally, there was a decline in ionic channel proteins related to neural plasticity, downregulation of ULK1

expression and activity essential for cellular autophagy, and a notable increase in the phosphorylation and polymerization levels of tau protein.

At present, although a number of studies have indicated that the dysfunction of Na_V channels is intimately associated with multiple neurological diseases, the specific mechanisms have consistently lacked in-depth exploration[2]. In this study, on the one hand, we conducted the inaugural assessment of the impacts of PoTX on the functions of neural cells, and ascertained that PoTX can trigger alterations in functional genes and proteins related to neural cell cycle, senescence and plasticity by activating Na^+ channels and causing an elevation in intracellular Ca^{2+} level. On the other hand, taking into account that PoTX possesses the nature of eliciting prolonged neural excitation and extensive alterations in cellular pathway activities without significantly impacting the viability of neural cells, we disclosed that PoTX is an ideal tool molecule for in-depth exploration of the functions of Na_V channels and the inherent connections among long-term pain, neurological disorders, changes in cognitive functions, and depression in the future, which holds considerable significance for comprehending the mechanisms of diseases and the development of therapeutic drugs.

Materials and methods

Reagent and materials

Poneratoxin (product number: HY-P10234), ouabain (HY-B0542), veratridine (HY-N6691) were purchased from MedChemExpress (USA). Tetrodotoxin was purchased from Taizhou Kangte Bioengineering Co., Ltd. (China). SH-SY5Y cells were purchased from the Pricella (China). DMSO (D8371) and penicillin-streptomycin liquid (100×, P1400) were purchased from Solarbio (China). Dulbecco's Modified Eagle Medium/Nutrient Mixture F-12 (DMEM/F12, 11320033), fetal bovine serum (FBS, 10099141 C), TRIzol™ reagent (15596018CN), SuperScript™ double-strand cDNA synthesis kit (11917020), RevertAid First Strand cDNA Synthesis Kit (K1622) were purchased from Thermo Fisher Scientific (USA). Cell counting kit-8 (FB29236) was purchased from FreeMoreBio (China). Fluo-4 calcium assay kit (S1061S), cell cycle and apoptosis analysis kit (C1052), RIPA lysis buffer (P0013B), phenylmethanesulfonyl fluoride (100 mM, ST506), protease and phosphatase inhibitor cocktail (P1045), BCA protein assay kit (P0012), SDS-PAGE sample loading buffer (P0015), primary antibody dilution buffer (P0023A) were purchased from Beyotime (China). Monoclonal anti-p-tau S396 (ab109390, 1:10000), anti-GSK-3 α/β (ab185141, 1:5000) and anti-p53 (ab32389, 1:10000) antibodies were purchased from Abcam (UK). Monoclonal anti-tau (43894, 1:1000), anti-pan Akt (4691, 1:1000), anti-p-Akt Ser473 (4060, 1:2000), anti-p-GSK-3 α Ser21 (9316, 1:1000), anti-p-GSK-3 β Ser9 (5558, 1:1000), anti-ULK1 (8054, 1:1000), anti-p-ULK1 Ser757 (6888, 1:1000) and anti-CDK5 (14145, 1:1000) antibodies were purchased from Cell Signaling Technology (USA). Monoclonal anti-β-actin (B1029, 1:5000) and anti-GAPDH (B3029, 1:5000) antibodies, peroxidase-conjugated anti-mouse secondary antibody (BF03001, 1:6000), peroxidase-conjugated anti-rabbit secondary antibody (BF03008, 1:6000) and enhanced/super ECL kit (BF06053) were purchased from Biodragon (Beijing, China). SDT lysis buffer (SL1029) was purchased from Coolaber (China). Multicolor prestained protein ladder (10–250 kDa, WJ103) was purchased from Shanghai Epizyme (China). TruSeq™ RNA Library Prep Kit v2 was purchased from Illumina (USA). NEBNext® Magnesium RNA Fragmentation Module was purchased from New England Biolabs (USA).

Cell culture

HEK293 cells stably expressing the human $hNa_V1.2$ or $hNa_V1.3$ were cultured on DMEM supplemented with 10% heatinactivated FBS, 50 μg/mL Hygromycin B in an incubator at 37 ℃ with 5% CO_2. The SH-SY5Y cells were cultured at 37 ℃ in a complete DMEM/F12 culture medium consisting of 15% FBS, supplemented with 100 units/ml penicillin and 0.1 mg/ml streptomycin at 37 °C under a humidified atmosphere of 5% CO_2. The ND7/23 cells were cultured at 37 ℃ in a complete RPMI-1640 culture medium consisting of 10% FBS, supplemented with 100 units/ml penicillin and 0.1 mg/ml streptomycin at 37 °C under a humidified atmosphere of 5% CO_2. The cells were routinely tested for mycoplasma contamination using the Myco-Lumi™ Luminescent Mycoplasma Detection Kit (Beyotime, C0298S), following the protocol outlined in the instructions. Cells that had undergone approximately 3 to 10 passages were utilized in this study.

Whole-cell voltage-clamp electrophysiology

Whole-cell patch-clamp experiments were performed using a AXON 700B electrophysiology platform (AXON, USA). The extracellular solution (ECS) contained 4 mM KCl, 2 mM $CaCl_2$, 1 mM $MgCl_2$, 10 mM HEPES, and 10 mM glucose (pH 7.4). The intracellular solution (ICS) contained 130 mM CsF, 10 mM NaCl, 10 mM EGTA and 10 mM HEPES (pH 7.2). Compounds were diluted in ECS with 0.1% DMSO. Voltage clamping and data acquisition were performed using pClamp software with a sampling rate of 10 kHz. Following the establishment of whole-cell recording, cells were held at − 100 mV, and a depolarizing pulse of 50 ms to -10 mV was applied to elicit sodium currents, followed by repolarization to -120 mV. This voltage protocol was repeated every 10 s (5 s for SH-SY5Y cells). Once the sodium current stabilized, drug application commenced. Compounds were administered in ascending order of concentration, starting from the lowest test concentration.

Assessment of cytotoxicity

Cell viability was measured though the CCK-8 assay. Briefly, cells were seeded in 96-well plates with a density of 2500 cells per well and cultured in 100 μL of complete medium for 24 h. Following this incubation period, the cells were treated with DMSO or specified compounds for indicated times. Subsequently, 10 μL of CCK-8 solution was added to each well, and the incubation continued for an additional 2 h.

Te absorbance at 450 nm was measured using TECAN Infinite E Plex multimode microplate reader at 25 °C. The cell viability percentage was calculated by.

$$Viability\,\% = \frac{OD_{test} - OD_{blank}}{OD_{negative} - OD_{blank}} \times 100\% \quad (1)$$

where the OD_{test} refers to the average absorbance value of wells treated with indicated compounds, OD_{blank} denotes the average absorbance value of wells devoid of cells, and $OD_{negative}$ represents the average absorbance value of wells treated with DMSO control based on three biological replicate.

Evaluation of intracellular calcium concentration

SH-SY5Y cells were seeded onto black 96-well cell culture plate at a density of 2000 cells per well. Following cell adhesion to the plate, the culture medium was removed, and 90 μL of Fluo-4 staining solution was added to each well. The plates were then incubated in the dark at 37 °C for 30 min. Prior to measuring intracellular calcium concentration, 10 μL of tenfold concentrated PoTX or an equivalent concentration of DMSO was introduced into each well. Fluorescence intensity was subsequently measured using a TECAN Infinite E Plex multimode microplate reader at 25 °C (Ex/Em = 490/525 nm).

Apoptosis analysis by flow cytometry

SH-SY5Y cells were seeded in 6-well plates and were treated with DMSO controls or indicated compounds for a duration of 24 h. Following the treatment, both non-adherent and adherent cells were harvested, and a cell cycle assay was conducted using the Cell Cycle and Apoptosis Analysis Kit in accordance with the manufacturer's instructions. The distribution of the cell phases was analyzed utilizing a CytoFlex Flow Cytometer (Beckman Coulter).

RNA extraction and library preparation

SH-SY5Y cells were seeded in 6-well plates and cultured until they reached approximately 70% confluency. Subsequently, the cells were treated with either 1 μM PoTX (designated as the Low group), 10 μM PoTX (designated as the High group), or DMSO (designated as the Control group) for a duration of 24 h. Three replicate wells were established for each treatment group. After treatment, the cells were harvested, and total RNA was extracted using TRIzol™ reagent. The quality of the RNA was assessed with Agilent Bioanalyzer 5300 and quantified using NanoDrop ND-2000 spectrophotometer. In the TTX blocking experiment, cells were initially incubated with 100 μM TTX for 5 min, followed by the addition of either DMSO or a indicated concentrations of PoTX to sustain the treatment of 24 h.

For each sample, 1 μg of total RNA (OD260/280 = 1.8–2.2; OD260/230 ≥ 2.0; RQN ≥ 6.5; 28 S:18 S ratio ≥ 1.0) was utilized to prepare the RNA-seq transcriptome library employing the TruSeq™ RNA Library Prep Kit v2. mRNA was separated by polyA selection using Oligo (dT) beads and fragmented into small pieces using NEBNext® Magnesium RNA Fragmentation Module. Then, double-stranded cDNA was constructed using SuperScript™ double-strand cDNA synthesis kit. The resulting cDNA was subsequently subjected to end-repair, phosphorylation, and adapter addition in accordance with the library construction protocol. Libraries were size-selected for cDNA target fragments of 300 bp and amplified through 15 cycles of PCR. Following quantification with Qubit 4.0.

Transcriptome analysis

The sequencing library was prepared on the Illumina NovaSeq X Plus platform (PE150) utilizing the NovaSeq Reagent Kit. The raw paired-end reads of sequencing were subjected to trimming and quality control using fastp with default parameters. The clean reads for each sample were aligned to the reference genome (Homo_sapiens, GRCh38) in orientation mode utilizing HISAT2 software. The mapped reads from each sample were then assembled through a reference-based approach employing StringTie. The expression level of each transcript was determined using the transcripts per million reads (TPM) method, and the RSEM software was employed to quantify gene abundances. The differential expression genes (DEGs) were identified using the DESeq2 software, applying the screening criteria of an adjusted P-value (P-adjust) < 0.05 and a Fold Change (FC) ≥ 2. The fastcluster software package was utilized for the clustering analysis of target genes. The Goatools tool was employed for Gene Ontology (GO) annotation and enrichment analysis, while KOBAS was used for the Kyoto Encyclopedia of Genes and Genomes (KEGG) analysis.

Quantitative real-time PCR analysis

SH-SY5Y or ND7/23 cells were cultured in 6-well plates and treated with either 1 μM or 10 μM PoTX, or a DMSO control, for 24 h. Total RNA was extracted using TRIzol™ reagent, and complementary DNA was synthesized from the extracted total RNA samples utilizing the RevertAid First Strand cDNA Synthesis Kit. Quantitative PCR analysis was conducted on the ABI StepOnePlus™ Real-Time PCR System. GAPDH served as the reference gene and relative fold changes of target genes in the expression levels were calculated using the $2^{-\Delta\Delta CT}$ method. Three replicates were analyzed in each group.

Total protein extraction and digestion

SH-SY5Y cells were exposed to DMSO (Control group) or PoTX at concentrations of 1 μM (Low group), 10 μM (High group) for a duration of 24 h. Each group consisted of three biologically independent samples. Following treatment, the samples were suspended in lysis buffer containing 1% sodium dodecyl sulfate (SDS), 8 M urea, and a protease inhibitor cocktail, and incubated on ice for 30 min. During this incubation period, the samples underwent ultrasonication for 2 min and vortexing for 10 s every five minutes. Upon centrifugation at 4 °C, 16,000*g* for 30 min, the protein concentration within the supernatant was measured by BCA protein assay kit. A total of 100 μg protein of protein were re-suspended in triethylammonium bicarbonate buffer (TEAB) at a

final concentration of 100 mM, followed by reduction with 10 mM tris(2-carboxyethyl)phosphine (TCEP) at 37 °C for 60 min. Thereafter, proteins were alkylated with iodoacetamide (IAM) at a concentration of 40 mM in darkness at room temperature for an additional duration of 40 min. The mixture was then centrifuged at 10,000*g* for 20 min at 4 °C. The resulting pellet was collected and subsequently re-suspended in 100 µL of TEAB of a final concentration of 100 mM. Trypsin was introduced to the solution at a 1:50 mass ratio of trypsin to protein and incubated overnight at 37 °C. Then, the samples were concentrated using a vacuum concentrator and re-solubilized in 0.1% trifluoroacetic acid (TFA). Following desalting with HLB, the digested protein products were dried and quantified utilizing the NANO DROP ONE (Thermo Scientific).

4D-DIA proteomic analysis

Digested protein products were separated by the Thermo Scientific Vanquish Neo UHPLC system which was directly interfaced with the Orbitrap Astral mass spectrometer. The analytical column was uPAC High Throughptu column (75 µm×5.5 cm, Thermo, USA). The mobile phase consisted of a mixture of phase A and B, in which phase A was composed of 2% acetonitrile and 0.1% formic acid in water, and phase B was composed of 80% acetonitrile and 0.1% formic acid in water. The Orbitrap Astral mass spectrometer was operated in the data-independent acquisition (DIA) mode with the scanning range of 100–1700 m/z.

The MS/MS spectra were searched against the selected database using the software Spectronaut software (Version 19). 6 peptides per protein and 3 daughter ions per peptide were selected for quantitative analysis. The parameters are as follows up : Protein FDR ≤ 0.01, Peptide FDR ≤ 0.01, Peptide Confidence ≥ 99%, XIC width ≤ 75ppm. Shared and modified peptides were excluded from the analysis, and peak areas were calculated and aggregated to produce the quantitative results. Only proteins associated with at least one unique peptide were considered for protein identification. The proteomic data was analyzed using the Majorbio Cloud platform (https://cloud.majorbio.com)[44]. The R package "t-test" was employed to calculate P-values and fold change (FC) for the proteins between two groups. FC ≥ 1.2 or ≤ 0.83 and p-value < 0.05 were regarded as the criteria for screening differentially expressed proteins (DEPs). Functional annotation of interest DEPs was performed using the GO (http://geneontology.org/) and KEGG pathway (http://www.genome.jp/kegg/).

Immunoblotting

SH-SY5Y or ND7/23 cells were harvested and inoculated into 6-well plates prior to treatment with PoTX for a duration of 24 h. Subsequently, the cells were lysed using RIPA lysis buffer supplemented with 1 mM phenylmethanesulfonyl fluoride, along with a protease and phosphatase inhibitor cocktail. The protein concentrations were quantified utilizing a BCA protein assay kit. Loading buffer was added to the lysates, which were then boiled at 95 °C before being resolved on SDS-PAGE and subsequently transferred onto polyvinylidene fluoride (PVDF) membranes. The blots were blocked for 2 h in blocking buffer (5% BSA in TBST) and incubated overnight at 4 °C with primary antibodies. Following three washes with TBST buffer, the blots were incubated for 2 h at room temperature with corresponding secondary antibodies in TBST containing 5% BSA. Chemiluminescence detection was performed using the Cytiva ImageQuant 800 system.

Data availability

The mass spectrometry proteomics data have been deposited to the ProteomeXchange Consortium via the PRIDE partner repository with the dataset identifier PXD060121. Reviewers can access the dataset by logging in to the PRIDE website with the username "reviewer_pxd060121@ebi.ac.uk" and password "S3aAkWqopH88". Sequence data that support the findings of this study have been deposited in the National Center for Biotechnology Information with the primary accession code PRJNA1215545. The data is accessible to reviewers upon request from the corresponding author. Moreover, it will be made publicly available online once the manuscript is published. Supporting Figs. S1–S5) and full western blots (S6–S14) were available in the Supporting Information.

Received: 22 January 2025; Accepted: 10 July 2025
Published online: 16 July 2025

References

1. Noreng, S., Li, T. & Payandeh, J. Structural pharmacology of voltage-gated sodium channels. *J. Mol. Biol.* **433**, 166967 (2021).
2. Barbieri, R., Nizzari, M., Zanardi, I., Pusch, M. & Gavazzo, P. Voltage-gated sodium channel dysfunctions in neurological disorders. *Life-Basel.* **13** (2023).
3. Catterall, W. A. Forty years of sodium channels: structure, function, pharmacology, and epilepsy. *Neurochem. Res.* **42**, 2495 (2017).
4. Alsaloum, M. et al. Voltage-gated sodium channels in excitable cells as drug targets. *Nat. Rev. Drug Discov.* **24**, 358 (2025).
5. Mantegazza, M., Curia, G., Biagini, G., Ragsdale, D. S. & Avoli, M. Voltage-gated sodium channels as therapeutic targets in epilepsy and other neurological disorders. *Lancet Neurol.* **9**, 413 (2010).
6. Ciccone, R. et al. Amyloid beta-induced upregulation of Na(v)1.6 underlies neuronal hyperactivity in Tg2576 alzheimer's disease mouse model. *Sci. Rep.-UK.* **9**, 13592 (2019).
7. Valentino, R. J. & Volkow, N. D. Untangling the complexity of opioid receptor function. *Neuropsychopharmacol.* **43**, 2514 (2018).
8. Schmidt, J. O. *The Sting of the Wild* (Johns Hopkins University, 2016).
9. Piek, T., Hue, B., Mantel, P., Nakajima, T. & Schmidt, J. O. Pharmacological characterization and chemical fractionation of the venom of the Ponerine ant, Paraponera clavata (F). *Comp. Biochem. Physiol. C Comp. Pharmacol. Toxicol.* **99**, 481 (1991).
10. Piek, T. et al. Poneratoxin, a novel peptide neurotoxin from the venom of the ant, Paraponera clavata. *Comp. Biochem. Physiol. C Comp. Pharmacol. Toxicol.* **99**, 487 (1991).
11. Duval, A., Malecot, C. O., Pelhate, M. & Piek, T. Poneratoxin, a new toxin from an ant venom, reveals an interconversion between two gating modes of the Na channels in frog skeletal muscle fibres. *Pflug Arch. Eur. J. Phys.* **420**, 239 (1992).
12. Robinson, S. D. et al. Ant venoms contain vertebrate-selective pain-causing sodium channel toxins. *Nat. Commun.* **14**, 2977 (2023).
13. Lopez-Suarez, L., Awabdh, S. A., Coumoul, X. & Chauvet, C. The SH-SY5Y human neuroblastoma cell line, a relevant in vitro cell model for investigating neurotoxicology in human: focus on organic pollutants. *Neurotoxicology.* **92**, 131 (2022).

14. Xicoy, H., Wieringa, B. & Martens, G. J. The SH-SY5Y cell line in Parkinson's disease research: a systematic review. *Mol. Neurodegener.* **12**, 10 (2017).
15. Zhang, Y. et al. Proteomics of plasma-derived extracellular vesicles reveals S100A8 as a novel biomarker for alzheimer's disease: A preliminary study. *J. Proteom.* **308**, 105279 (2024).
16. Peng, Y. et al. Neuroinflammatory in vitro cell culture models and the potential applications for neurological disorders. *Front. Pharmacol.* **12**, 671734 (2021).
17. Voogd, E., Frega, M. & Hofmeijer, J. Neuronal responses to ischemia: scoping review of insights from human-derived in vitro models. *Cell Mol. Neurobiol.* **43**, 3137 (2023).
18. Vetter, I. et al. Characterisation of Na(v) types endogenously expressed in human SH-SY5Y neuroblastoma cells. *Biochem. Pharmacol.* **83**, 1562 (2012).
19. Lee, J., Kim, S., Kim, H., Kim, H. J. & Yu, F. H. NaV1.6 and NaV1.7 channels are major endogenous voltage-gated sodium channels in ND7/23 cells. *PLoS One.* **14**, e221156 (2019).
20. Patmore, L., Duncan, G. P. & Spedding, M. The effects of calcium antagonists on calcium overload contractures in embryonic chick myocytes induced by Ouabain and veratrine. *Br. J. Pharmacol.* **97**, 83 (1989).
21. Wu, H., He, P. & Jia, R. Effects of micro-Conotoxin GIIIB on the cellular activity of mouse skeletal musculoblast: combined transcriptome and proteome analysis. *Proteome Sci.* **21**, 17 (2023).
22. Lingrel, J. B. & Kuntzweiler, T. Na+,K(+)-ATPase. *J. Biol. Chem.* **269**, 19659 (1994).
23. Manger, R. L., Leja, L. S., Lee, S. Y., Hungerford, J. M. & Wekell, M. M. Tetrazolium-based cell bioassay for neurotoxins active on voltage-sensitive sodium channels: semiautomated assay for saxitoxins, brevetoxins, and ciguatoxins. *Anal. Biochem.* **214**, 190 (1993).
24. Wang, S. Y. & Wang, G. K. Voltage-gated sodium channels as primary targets of diverse lipid-soluble neurotoxins. *Cell. Signal.* **15**, 151 (2003).
25. Zhang, X. Y., Bi, R. Y., Zhang, P. & Gan, Y. H. Veratridine modifies the gating of human voltage-gated sodium channel Nav1.7. *Acta Pharmacol. Sin.*. **39**, 1716 (2018).
26. Murakami, M. & Kudo, I. Phospholipase A2. *J. Biochem.* **131**, 285 (2002).
27. Saha, S., Bose, R., Chakraborty, S. & Ain, R. Tipping the balance toward stemness in trophoblast: Metabolic programming by Cox6B2. *FASEB J.* **36**, e22600 (2022).
28. Schaeffer, E. L., Da, S. E., Novaes, B. A., Skaf, H. D. & Gattaz, W. F. Differential roles of phospholipases A2 in neuronal death and neurogenesis: implications for alzheimer disease. *Prog. Neuro-Psychoph.* **34**, 1381 (2010).
29. Arnold, S. Cytochrome c oxidase and its role in neurodegeneration and neuroprotection. *ADV. EXP. MED. BIOL.* **748**, 305 (2012).
30. Yin, C., Harms, A. C., Hankemeier, T., Kindt, A. & de Lange, E. C. M. Status of metabolomic measurement for insights in Alzheimer's disease progression-what is missing? *Int J. Mol. Sci* **24** (2023).
31. Makarova, M., Rycek, L., Hajicek, J., Baidilov, D. & Hudlicky, T. Tetrodotoxin: history, biology, and synthesis. *Angew. Chem. Int. Edit.* **58**, 18338 (2019).
32. Gomez, D. S. J. N. et al. Glutamate receptor 4 as a fluid biomarker for the diagnosis of psychiatric disorders. *J. Psychiatr. Res.* **156**, 390 (2022).
33. Silva, F. R. et al. N-type Ca(2+) channels are affected by full-length mutant Huntingtin expression in a mouse model of huntington's disease. *Neurobiol. Aging.* **55**, 1 (2017).
34. Hidalgo, S., Campusano, J. M. & Hodge, J. The Drosophila ortholog of the schizophrenia-associated CACNA1A and CACNA1B voltage-gated calcium channels regulate memory, sleep and circadian rhythms. *Neurobiol. Dis.* **155**, 105394 (2021).
35. Yang, L. G., March, Z. M., Stephenson, R. A. & Narayan, P. S. Apolipoprotein E in lipid metabolism and neurodegenerative disease. *Trends Endocrin. Met.* **34**, 430 (2023).
36. Anand, A. A., Khan, M., V, M. & Kar, D. The molecular basis of Wnt/beta-catenin signaling pathways in neurodegenerative diseases. *Int. J. Cell Biol.* **2023**, 9296092 (2023).
37. Bramblett, G. T. et al. Abnormal Tau phosphorylation at Ser396 in alzheimer's disease recapitulates development and contributes to reduced microtubule binding. *Neuron.* **10**, 1089 (1993).
38. Johnson, G. V. & Stoothoff, W. H. Tau phosphorylation in neuronal cell function and dysfunction. *J. Cell. Sci.* **117**, 5721 (2004).
39. Cross, D. A., Alessi, D. R., Cohen, P., Andjelkovich, M. & Hemmings, B. A. Inhibition of glycogen synthase kinase–3 by insulin mediated by protein kinase B. *Nature.* **378**, 785 (1995).
40. Srivastava, A. K. & Pandey, S. K. Potential mechanism(s) involved in the regulation of glycogen synthesis by insulin. *Mol. Cell. Biochem.* **182**, 135 (1998).
41. Jacinto, E. et al. SIN1/MIP1 maintains rictor-mTOR complex integrity and regulates Akt phosphorylation and substrate specificity. *Cell.* **127**, 125 (2006).
42. Chan, E. Y., Kir, S. & Tooze, S. A. SiRNA screening of the Kinome identifies ULK1 as a multidomain modulator of autophagy. *J. Biol. Chem.* **282**, 25464 (2007).
43. Wang, Y. et al. The role of cellular senescence in neurodegenerative diseases. *Arch. Toxicol.* **98**, 2393 (2024).
44. Han, C. et al. Majorbio Cloud 2024: Update single-cell and multiomics workflows. *Imeta.* **3**, e217 (2024). (2024).

Acknowledgements

This work was generously supported by State Key Laboratory of Chemistry for NBC Hazards Protection of China (SKLNBC2023-05).

Author contributions

F.M. conceived the project and designed the study. Z.L. and X.D. performed the biological experiments. J.X. and M.Z. analyzed data. Z.L. wrote the manuscript with contributions from all authors, and Y.G. and Z.G. edited the final manuscript.

Declarations

Competing interests

The authors declare no competing interests.

Additional information

Supplementary Information The online version contains supplementary material available at https://doi.org/10.1038/s41598-025-11459-z.

Correspondence and requests for materials should be addressed to F.M.